IEEE Access
Multidisciplinary ⋮ Rapid Review ⋮ Open Access Journal

Received September 5, 2018, accepted September 26, 2018, date of publication October 1, 2018, date of current version October 19, 2018.

Digital Object Identifier 10.1109/ACCESS.2018.2872936

Embedding WFRFT Signals Into TDCS for Secure Communications

XINYU DA[1], YUAN LIANG[2], HANG HU[2], RUIYANG XU[2], LEI NI[2], DONG ZHAI[2], AND YU PAN[2]
[1]Yango University, Fuzhou, Fujian 350000, China
[2]Air Force Engineering University, Xi'an 710077, China

Corresponding author: Yuan Liang (lycrazy0925@163.com)

This work was supported in part by the National Natural Science Foundation Program of China under Grant 61271250 and Grant 61571460 and in part by the National Postdoctoral Program for Innovative Talents under Grant 201700108.

ABSTRACT This paper presents a novel combinatory strategy to embed weighted-type fractional Fourier transform (WFRFT) precoding signals into transform domain communication system (TDCS). The original data can be divided into two parts. One part is modulated with the cyclic code shift keying in the traditional TDCS. The other part is first disguised as other higher order baseband modulations MPSK through WFRFT proceding process, then will further be embedded into the traditional TDCS system. A double-random scheme is designed to dynamically generate the pseudo phase for WFRFT rotation and TDCS basic function's phase. Theoretical analyses show that the higher spectral efficiency can be obtained while causing little effect on its original communication quality. The final simulations demonstrate that the constellation precoding method can help disguise the original signals into other higher order baseband PSK modulations with a controllable Gaussian-like noise. Besides, owing to the dynamically double-random phase generation scheme, the proposed combinatory WFRFT-TDCS system can gain better anti-eavesdropping capacity while maintaining its own communications' quality with regards to bit error rate performances.

INDEX TERMS Weighted-type fractional Fourier transform (WFRFT) precoding, embedded transform domain communication system (TDCS), double-random phase, anti-eavesdropping.

I. INTRODUCTION

Nowdays, wireless communication is more widely used in our daily life, and also becomes more and more indispensable owing to its convenience and being almost free of the space and time constraints. Especially, the developing 5G wireless technology enjoys unprecedented opportunities and exhibits promising prospects [1], [2]. Meanwhile, because of its inherent properties, i.e. broadcast nature, information disclosure and high deployment densities, wireless communication is vulnerable and easily suffer an unexpected attack or interception by other unauthorized receivers with the radio coverage. To guarantee the communication's security, the traditional cryptography-based method is employed and focuses mainly on the network layer or other upper layers in the open system interconnection (OSI) system. However, as for the cryptography-based systems, the distribution and maintenance of the secret key become more and more difficult to be implemented and subsequently make the secret key more vulnerable to malicious attacks [3]. Recently, as an important alternative to the cryptography-based methods, physical layer (PHY) has gained considerable concerns, mainly because it is implemented on the bottom layer and doesn't rely on the upper wireless links. Especially, when the device's power is low, PHY scheme security needn't consume significant overhead and can still well guarantee the system's security [4].

Traditionally, the spread spectrum (SS) based system has been proved a practical technology to guarantee both the communication quality and security [5], [6]. Meanwhile, considering more and more new intercepting technologies and methods are provided, the original transmitting signal becomes less reliable and easier to be captured or exploited when the communication system utilizes only the SS technology. Hence, new PHY strategies are necessarily adopted to further guarantee the communication security. As a novel time-frequency domain analyzing tool, weighted-type fractional Fourier transform (WFRFT) was first put forward by Shih [7]. Then, Mei *et al.* provided a hybrid carrier (HC) system based on WFRFT, and also proved that HC could be a promising strategy that can improve both the communication security and quality because of its time-frequency domain distribution property [8], [9]. Besides, because the

Gaussian-like components of WFRFT signals can serve as an artificial noise for the eavesdropper while causing no degradation on the authorized users [10], [11], WFRFT has also been proved to be an effective technology on PHY security communication. The traditional single-parameter WFRFT (SP-WFRFT) has only one parameter, namely, WFRFT order α. To some extent, the SP-WFRFT processed signal will exhibit constellation splitting and Gaussian-like properties with different α selections. According to [12], other more parameters will also affect the WFRFT modulated signals' characteristics. Unlike the SP-WFRFT, the MP-WFRFT has a much more complicated constellation mapping criterion and can help reduce the probability that the eavesdroppers attempt to grab the accurate parameter set by scanning the parameters [13], [14]. To make full use of SS and WFRFT technology, Qiu proposed a hybrid carrier direct spread code division multiple access (HC-DS-CDMA) and a hybrid carrier code division multiple access (HC-CMDA) system to combine the traditional spread spectrum with WFRFT, and proved the combinatory structure can achieve a better bit error rate (BER) performance over the narrowband interference (NBI) and additive white Gaussian noise (AWGN) channels.

In view of the fact that transform domain communication system (TDCS) was put forward in cognitive radio (CR) scenarios by German [15], and can be regarded as a spread spectrum technology to some extent [16]. Especially, when the cyclic code shift keying (CCSK) modulations are implemented, TDCS can well be compatible with the traditional orthogonal frequency division multiplexing (OFDM) scheme [17], [18]. Compared with the traditional SS technology, TDCS can enhance the system's anti-NBI ability by properly designing the magnitude of the basic function (BF). In addition, the BF vector can make the original signal behave like a Gaussian noise, which can further protect the system from being detected by other unauthorized receivers through the energy-based or statistic-based deletion methods.

Based on the above theories, it's tempting to design the combinatory WFRFT-TDCS system to make full use of the properties of TDCS and WFRFT. In the combinatory system of this paper, a novel combinatory structure is proposed to embed MP-WFRFT processed signals into TDCS based system. To overcome the multi-level values of the MP-WFRFT signals and be well compatible with TDCS, by properly selecting the parameter set $[\alpha, \boldsymbol{V}]$, we design the MP-WFRFT precoding method to make the MP-WFRFT processed signals to disguise as a higher order baseband modulation MPSK($M > 4$) with a controllable Gaussian-like noise. Besides, the double-random pseudo phase generation scheme is designed to dynamically generate the BF's phase of TDCS and rotating phase of MP-WFRFT. The MP-WFRFT precoding strategy and the double-random phase generation scheme can effectively assist the traditional TDCS system to improve its communication security.

This paper will be organized as follows: In Section 2, we elaborate the definition and basic properties of MP-WFRFT. In Section 3, by designing the combinatory WFRFT-TDCS system, we take deep analyses on the MP-WFRFT precoding method and double-random phase generation scheme. In Section 4, we analyze the theoretical performances on the power spectral density (PSD), spectral efficiency, anti-AWGN and anti-eavesdropping capacities. In Section 5, we conduct numerical simulations to evaluate the performances of the proposed system. Conclusions and future works are drawn in the final section.

II. WEIGHTED-TYPE FRACTIONAL FOURIER TRANSFORM

Considering the basic definition and properties of MP-WFRFT are frequently used in the theoretical derivations and related performance analyses in other sections, in this section, we will elaborate the definition and properties for MP-WFRFT in detail.

A. DEFINITION OF MP-WFRFT

Let $\boldsymbol{x}_0$ be the arbitrary complex baseband signals, and the vector form of $\boldsymbol{x}_0$ is $\boldsymbol{x}_0 = [x_{0,0}, x_{0,1}, \cdots x_{0,N-1}]^{\mathrm{T}} \in \mathbb{C}$, where $\mathbb{C}$ denotes the set of complex numbers. Then the MP-WFRFT of $\boldsymbol{x}_0$ can be defined as [12]

$$T_M^{\alpha,\boldsymbol{V}} \rightarrow \boldsymbol{W}_M^{\alpha,\boldsymbol{V}}(\boldsymbol{x}_0) = \sum_{l=0}^{M-1} \omega_l(\alpha, \boldsymbol{V}) \boldsymbol{F}_N^{4l/M} \boldsymbol{x}_0 \tag{1}$$

where M denotes the number of basic operators, and $M \geq 4$; $\boldsymbol{F}_N$ denotes the normalized discrete Fourier transform(DFT) matrix, and the (u, v)-th element is $F_N(u,v) = (1/\sqrt{N}) \exp(-\mathrm{j}2\pi uv/N)$, $u, v = 0, 1, \cdots, N-1$.

Moreover, as for Eq.(1), $\omega_l(\alpha, \boldsymbol{V})$, $l = 0, 1, \cdots, M-1$ denote the corresponding weighting coefficients, whose expressions are given by

$$\omega_l(\alpha, \boldsymbol{V}) = \frac{1}{M} \sum_{h=0}^{M-1} \exp\left\{ \pm \frac{\mathrm{j}2\pi}{M} \left[\begin{array}{c} \alpha\,(Mm_h + 1) \cdot \\ (Mn_h + h) - lh \end{array} \right] \right\} \tag{2}$$

In Eq.(2), α is the transform order of MP-WFRFT; m_h, m_h are the extension parameter derivated from the transform periodicity, and $\boldsymbol{MV} = [m_0, m_1, \cdots, m_{M-1}]$, $\boldsymbol{NV} = [n_0, n_1, \cdots, n_{M-1}]$, and $\boldsymbol{V} = [\boldsymbol{MV}, \boldsymbol{NV}]$. Then $[\alpha, \boldsymbol{V}]$ can be regarded as the MP-WFRFT parameter set.

B. PROPERTIES OF MP-WFRFT

According to [12], the MP-WFRFT operator $T_M^{\alpha,\boldsymbol{V}}$ in Eq.(1) should satisfies the following four requirements

- Continuity postulate: $\omega_l(\alpha, \boldsymbol{V})$, $l = 0, 1, \cdots, M-1$ are continuous for the fraction order α.
- Boundary postulate: $\omega_l(n, \boldsymbol{V}) = \delta(n-l)$, $0 \leq n, l \leq M-1$.
- Periodicity postulate: $\omega_l(\alpha, \boldsymbol{V}) = \omega_l(\alpha + M, \boldsymbol{V})$, $0 \leq l \leq M-1$, for every choice of the order α.
- Additive postulate: for every choice of the order α and β, $T_M^{\alpha,\boldsymbol{V}}$ has the following property, $T_M^{\alpha,\boldsymbol{V}} T_M^{\beta,\boldsymbol{V}} = T_M^{\beta,\boldsymbol{V}} T_M^{\alpha,\boldsymbol{V}} = T_M^{\alpha+\beta,\boldsymbol{V}}$.

According to the continuity and periodicity postulates, we can deduce that WFRFT order α is a real number, namely, $\alpha \in \mathbb{R}$, where $\mathbb{R}$ denotes the set of real numbers; besides, α has the period of M. Then we can constrain α in the range $[0, M)$. To satisfy the boundary postulate, as for the extension parameters $\boldsymbol{V}$, each element in $\boldsymbol{V}$ should be integer, then m_h, $m_h \in \mathbb{Z}$, where $\mathbb{Z}$ denotes the set of integer numbers.

Moreover, according to additive postulate, $T_M^{\alpha,\boldsymbol{V}} T_M^{\beta,\boldsymbol{V}} = T_M^{\beta,\boldsymbol{V}} T_M^{\alpha,\boldsymbol{V}} = T_M^{\alpha+\beta,\boldsymbol{V}}$, when $\alpha = -\beta$, combining with the definition of MP-WFRFT in Eq.(1), then, $T_M^{\alpha,\boldsymbol{V}} T_M^{\beta,\boldsymbol{V}} = T_M^{\alpha+\beta,\boldsymbol{V}} = T_M^{0,\boldsymbol{V}}$. We can infer that the original transmitting signal can be fully recovered through the MP-WFRFT (with order α) and the inverse MP-WFRFT (with order $-\alpha$) operators. We mainly considering the situation where $M = 4$ owing to the fact that the MP-WFRFT based system can be well compatible with the traditional single carrier(SC) and multi-carrier(MC) systems. In addition, the analysis process and related conclusions can also are similar with the situations where $M > 4$. Thus, this paper focuses mainly on the multiple-parameter 4-WFRFT (MP-4-WFRFT). For clarity's sake, we will skip the prefix and use WFRFT for short in the following parts. Considering the normalized DFT matrix $\boldsymbol{F}_N$ has the property, $\boldsymbol{F}_N^0 = \boldsymbol{I}_N$, $\boldsymbol{F}_N^2 = \boldsymbol{T}_N$, $\boldsymbol{F}_N^3 = \boldsymbol{T}_N\boldsymbol{F}_N$. When $M = 4$, the expression of Eq.(1) can be rewritten as

$$\begin{aligned} \boldsymbol{W}_4^{\alpha,\boldsymbol{V}} &= \omega_0(\alpha, \boldsymbol{V})\boldsymbol{F}_N^0 + \omega_1(\alpha, \boldsymbol{V})\boldsymbol{F}_N^1 \\ &\quad + \omega_2(\alpha, \boldsymbol{V})\boldsymbol{F}_N^2 + \omega_3(\alpha, \boldsymbol{V})\boldsymbol{F}_N^3 \\ &= \omega_0(\alpha, \boldsymbol{V})\boldsymbol{I}_N + \omega_1(\alpha, \boldsymbol{V})\boldsymbol{F}_N^1 \\ &\quad + \omega_2(\alpha, V)\boldsymbol{T}_N + \omega_3(\alpha, \boldsymbol{V})\boldsymbol{T}_N\boldsymbol{F}_N \end{aligned} \tag{3}$$

where $\omega_l(\alpha, \boldsymbol{V})$, $l = 0, 1, 2, 3$ corresponds Eq.(2); and $\boldsymbol{T}_N$ denote the inverse matrix, whose expression is given by

$$\boldsymbol{T}_N = \begin{bmatrix} 1 & 0 & \cdots & 0 & 0 & 0 \\ 0 & 0 & \cdots & 0 & 0 & 1 \\ 0 & 0 & \cdots & 0 & 1 & 0 \\ \vdots & \cdots & 0 & \ddots & 0 & 0 \\ 0 & 0 & 1 & 0 & \cdots & 0 \\ 0 & 1 & 0 & 0 & \cdots & 0 \end{bmatrix}_{N\times N} \tag{4}$$

According to Eq.(3), the basic WFRFT process can be implemented as Fig. 1. In Fig. 1, the MP-WFRFT signals consist of four parts. The first part with coefficient $\omega_0(\alpha, \boldsymbol{V})$ and the third one with coefficient $\omega_2(\alpha, \boldsymbol{V})$ are the time domain signal; the second and fourth ones with coefficients $\omega_1(\alpha, \boldsymbol{V})$ and $\omega_3(\alpha, \boldsymbol{V})$ respectively are the frequency domain signal. The time domain signal superposition is related to the constellation rotation and splitting characteristics. And the frequency domain signal determine the system's quasi-Gaussian characteristics mainly because that the random time-domain signals with DFT process approximately obey the Gaussian distribution [19], [20].

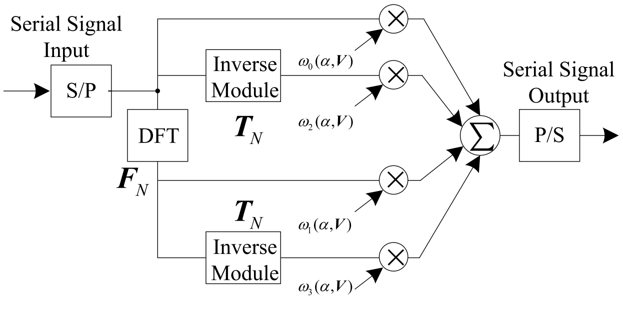

FIGURE 1. Implementation structure of WFRFT.

According to the MP-WFRFT's implementation process in Fig. 1, we need only one DFT module and two inverse modules. As for the MP-WFRFT based system with the block length N, through the fast algorithm, Fast Fourier Transform (FFT), DFT can be implemented with the calculation complexity $\mathcal{O}(N\log_2(N))$, and the Inverse module doesn't incur other addition or multiplying operations. In addition, As shown in Eq.(3), another $4N$ multiplying operations are needed when implementing MP-WFRFT. Thereby, the MP-WFRFT process needs $\mathcal{O}(4N + N\log_2(N))$ operations. Compared with the FFT process, the MP-WFRFT process would bring a negligible computational burden, which makes that the MP-WFRFT can be easily implemented in the practical communication applications.

III. SYSTEM'S DESCRIPTIONS

When an unauthorized user tries to eavesdrop the authorized transmitting signals, the eavesdropping process can be categorized into three steps: (i) Detection; (ii) Interception; (iii) Exploitation.

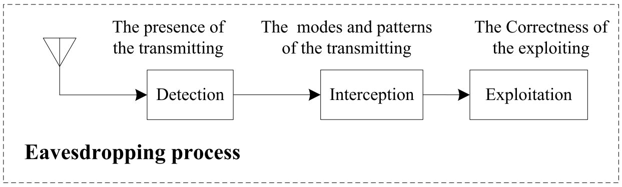

FIGURE 2. Three steps of the eavesdropping process.

As shown in Fig. 2, the threat model can be built as the three steps in eavesdropping process. As for the Eavesdropping process, first, the unauthorized user should try to detect the presence of the transmission; then, when the presence has been confirmed, the modulation modes or other signal processing methods should be recognized or recovered to help the unauthorized user capture the transmitting signal properly; last, after the transmitting signal has been detected and captured, the modulation parameters or encrypting strategies should be correctly obtained to finally exploit the original transmitting signal.

Thus, according to the three eavesdropping steps mentioned-above, we build our following combinatory WFRFT-TDCS structure based on the following reasons: the BF sequence in TDCS can serve as a spread spectrum sequence to some extent and make the original signal behave like Gaussian-like noise, which will make it quite difficult to be detected by other unauthorized receivers through traditional energy-based and statistics-based detection methods. Besides, WFRFT technology can disguise the original

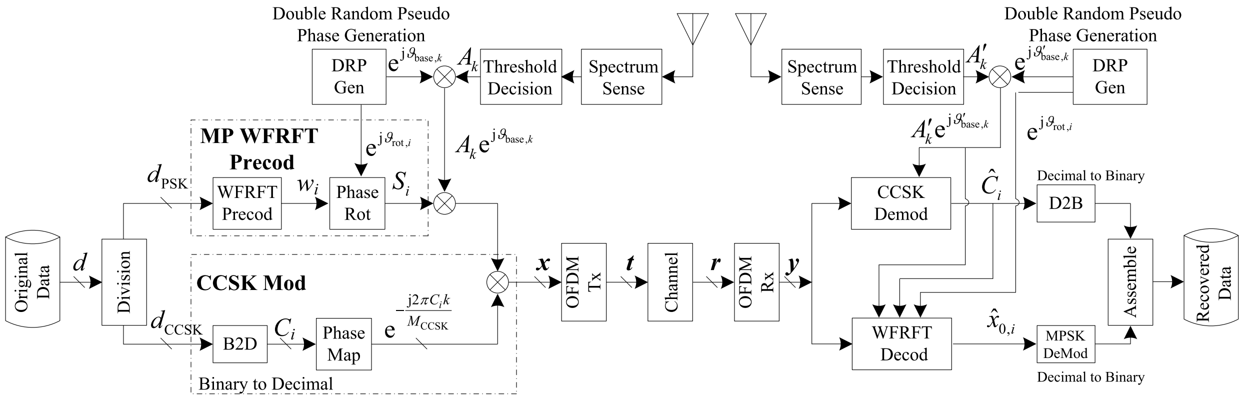

FIGURE 3. Architecture of the combinatory WFRFT-TDCS system.

baseband constellations into other higher modulations with a power-controllable Gaussian-like noise. Then, WFRFT processing constellations can prevent the transmitting signal from being intercepted by the constellation-based recognition methods. That is, the constellation patterns are quite difficult to be recognized by unauthorized users. What's more, the pseudo periodicity of the BF sequence in TDCS and the parameter diversity of modulation parameter set $[\alpha, \boldsymbol{V}]$ in WFRFT can cost the unauthorized user a large mount of time to correctly crack, then the BF sequence and WFRFT parameter set $[\alpha, \boldsymbol{V}]$ both can serve as an encrypting key to protect the authorized communication system from being exploited.

In this Section, we will illustrate our combinatory WFRFT-TDCS architecture and analyze some significant modules in detail, namely, WFRFT Precod module, Pseudo phase generation, Combinatory Demodulation in receiver.

A. COMBINATORY WFRFT-TDCS STRUCTURE

Fig. 3 depicts the overall structure of the proposed system. For clarity's sake, we use the notation Tx and Rx to denote the transmitting and receiving parts respectively. In Fig. 3, first, as for Tx, the original signal is d divided into two parts d_{PSK} and d_{CCSK}: one part d_{PSK} is MPSK-modulated into $\boldsymbol{x}_0$, then through WFRFT Precod, $\boldsymbol{x}_0$ can be further transformed into $\boldsymbol{w}$. Combining with the rotation phase $\boldsymbol{p}_{\text{rot}}$ $(p_{\text{rot},i} = e^{j\vartheta_{\text{rot},i}})$, the final WFRFT precoding signals $\boldsymbol{S}$ $(\boldsymbol{S} = [S_0, S_1, \cdots, S_{N-1}]^{\text{T}})$ can further serves as the embedded signal into the traditional TDCS; the other part d_{CCSK} is modulated by cyclic code shift keying(CCSK) on the traditional TDCS. By embedding WFRFT processing signals into the traditional TDCS, the original transmitting signal is encrypted and the system's communication's security can be guaranteed. Then, the combinatory signal $\boldsymbol{t}$ is transmitted through AWGN channel. Finally, as for Rx, there exists corresponding parts for the demodulation of C_i and $x_{0,i}$. In the following subsections, we will make elaborate analyses about the WFRFT Precod module, the double-random sequence Gen and the related demodulation scheme.

B. WFRFT PRECOD

In this subsection, we mainly analyze how BPSK signals can be disguised into MPSK signals. The precoding process and analysis method can be well expanded in other higher order PSK modulations (MPSK, $M > 2$). Through WFRFT process, BPSK signals can first be transformed into quasi-4PSK signals. Then, by rotating the constellation phase randomly, the quasi-4PSK can be further disguised into quasi-MPSK signals. In the following paragraph and figures, we often omit the parameter set vector $(\alpha, \boldsymbol{V})$ in $\omega_l(\alpha, \boldsymbol{V})$, $(l = 0,\ 1,\ 2,\ 3)$ and used the short notation ω_l, $(l = 0,\ 1,\ 2,\ 3)$ for the description's clarity.

Let $\boldsymbol{x}_1$, $\boldsymbol{x}_2$ and $\boldsymbol{x}_3$ be the 1-3 times DFT of $\boldsymbol{x}_0$. Based on Eq.(3), the WFRFT of $\boldsymbol{x}_0$ can be given by

$$\begin{aligned} \boldsymbol{W}_M^{\alpha,\boldsymbol{V}}(\boldsymbol{x}_0) &= \omega_0\boldsymbol{x}_0 + \omega_1\boldsymbol{x}_1 + \omega_2\boldsymbol{x}_2 + \omega_3\boldsymbol{x}_3 \\ &= (\omega_0\boldsymbol{F}_N^0 + \omega_1\boldsymbol{F}_N^1 + \omega_2\boldsymbol{F}_N^2 + \omega_3\boldsymbol{F}_N^3)\boldsymbol{x}_0 \\ &= (\omega_0\boldsymbol{I}_N + \omega_1\boldsymbol{F}_N + \omega_2\boldsymbol{T}_N + \omega_3\boldsymbol{F}_N^{-1})\boldsymbol{x}_0 \quad (5) \end{aligned}$$

in Eq.(5), $\boldsymbol{x}_0$ and $\boldsymbol{x}_2$ can be regarded as the time-domain signals and the corresponding superposition $\omega_0\boldsymbol{x}_0 + \omega_2\boldsymbol{x}_2$ is directly related to the constellation rotation and splitting (constellation-splitting characteristic); $\boldsymbol{x}_3$ and $\boldsymbol{x}_1$ are the DFT of $\boldsymbol{x}_2$ and $\boldsymbol{x}_0$ respectively. Considering that DFT is a linear transformation and the DFT of random time-domain signal is closely related to Gaussian noise (constellation-blurring characteristic), then $\boldsymbol{x}_0$ and $\boldsymbol{x}_2$ can be regarded as the frequency-domain signals and the combination of $\omega_1\boldsymbol{x}_1$ and $\omega_3\boldsymbol{x}_3$ can simply be regarded as the Gaussian-like signals. So we mainly focus on the constellation-splitting characteristic in MP-WFRFT Precod module, and more attention should be paid to the first $(\omega_0\boldsymbol{x}_0)$ and third $(\omega_2\boldsymbol{x}_2)$ parts rather than the second and fourth parts(corresponding the constellation-blurring characteristic) in Eq.(5). And the second$(\omega_1\boldsymbol{x}_1)$ and fourth$(\omega_3\boldsymbol{x}_3)$ ones can be simply regarded as the quasi-Gaussian noise.

1) BPSK→4PSK

According to the analysis in Fig. 1, the WFRFT based system's constellation splitting is related to the time domain signals ($\omega_0\boldsymbol{x}_0 + \omega_2\boldsymbol{x}_2$), while the constellation blurring is attributed to the frequency domain signals ($\omega_1\boldsymbol{x}_1 + \omega_3\boldsymbol{x}_3$).

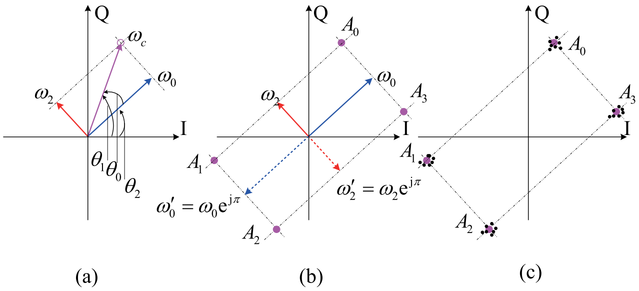

FIGURE 4. Geometry analysis model of BPSK→4PSK through WFRFT process. (a) Composition of ω_0 and ω_2. (b) Constellation-splitting caused by $\omega_0 x_0$ and $\omega_2 x_2$. (c) Geometry analysis model of BPSK→4PSK through WFRFT process.

To get an intuitive analysis on the constellation-splitting characteristic, in an inverse vision, we take the coefficients ω_0 and ω_2 as the basic vector, and take $\boldsymbol{x}_0$ and $\boldsymbol{x}_2$ as the weighting factors. Then, through geometry analysis, the signal superposition of $\omega_0\boldsymbol{x}_0$ and $\omega_2\boldsymbol{x}_2$ can be illustrated in Fig. 4. Fig. 4(a) depicts the basic model of the composition of ω_0 and ω_2, and ω_c is the corresponding composition vector. Considering ($\boldsymbol{x}_0$,$\boldsymbol{x}_2$) has four possible values, namely, (1, 1), (1, −1), (−1, 1) and (−1, −1), when the weighting factors $\boldsymbol{x}_0$ and $\boldsymbol{x}_2$ are added, there are totally four different compositions, as shown in Fig. 4(b). Besides, when the quasi-Gaussian noise ($\omega_1\boldsymbol{x}_1 + \omega_3\boldsymbol{x}_3$) are considered, the final constellation after WFRFT process are depicted in Fig. 4(c). In Fig. 4(a), for description's clarity, we define θ_1 and θ_2 as the phases of the vector ω_0 and ω_c respectively. Then the angle θ_0 between vector ω_0 and ω_c can be calculated by $\theta_0 = \langle\omega_0, \omega_c\rangle = \theta_1 - \theta_2$, where $\langle\cdot\rangle$ is the operation to obtain the angles.

Considering that the constellation of stand baseband signals are uniformly distributed in the X-Y axis, we should have the following angle and magnitude constraints:

- angle:
  ω_0 should be perpendicular to $\omega_2(\omega_0 \perp \omega_2)$, that is $\langle\omega_0, \omega_2\rangle = 90°$; Besides, in order to get a constellation distribution centered on X and Y axes, the angle of ω_2 (θ_2) should be forced to be parallel to X or Y axes, that is θ_2 should be forced to 0° or 90°.
- magnitude:
  Through WFRFT process, the disguising constellation should mainly exhibit the constellation-splitting characteristics, then the magnitude of ω_1 and ω_3 ($|\omega_1| + |\omega_3|$) should be confined to a small limit. Besides, the magnitude ratio of ω_2 to $\omega_0(|\omega_2|/|\omega_0|$) has a direct influence on the neighboring distance of different constellation points.

In fact, as for the constellation splitting process(BPSK→ 4PSK) in Fig. 4, the four constellation splitting points can be distributed uniformly on a unit circle only when $|\omega_2| = |\omega_0|$. For other coefficient magnitude ratios ($|\omega_2|/|\omega_0| \neq 1$), in a matter of clarity, we still regard the WFRFT precoding constellations as the 4PSK baseband constellations.

Based on the basic angle and magnitude constraints mentioned above, to disguise BPSK into 4PSK, we can build the related optimal model as follows

$$\begin{cases} \min f(\alpha, \boldsymbol{V}) = \sqrt{|\omega_2 \exp(j\pi/2) - \lambda\omega_0|^2} + \sqrt{|\omega_1|^2 + |\omega_3|^2} \\ s.t.\ \omega_l(\alpha, \boldsymbol{V}) = \dfrac{1}{4}\displaystyle\sum_{h=0}^{3} \exp\left\{\dfrac{j2\pi}{4}\left[(4m_h+1)\,\alpha\,(4n_h+1) - lh\right]\right\}, \\ \quad l = 0, 1, 2, 3; \\ \quad \boldsymbol{V} = [m_0, m_1, m_2, m_3, n_0, n_1, n_2, n_3]; \\ \quad |\omega_0(\alpha, \boldsymbol{V})| > \delta_1;\ |\omega_2(\alpha, \boldsymbol{V})| > \delta_2; \\ \quad \max(|\omega_1(\alpha, \boldsymbol{V})|, |\omega_3(\alpha, \boldsymbol{V})|) < \delta_3; \\ \quad m_h, n_h \in \mathbb{Z}^+, h = 0, 1, 2, 3; \\ \quad \alpha \in [0, 4), \alpha \in \mathbb{R}. \end{cases} \tag{6}$$

In Eq.(6), we design the object function based on the coefficient ratio($|\omega_2|/|\omega_0|$) and the quasi-Gaussian coefficient magnitude $|\omega_1|$ and $|\omega_3|$. We also set the related angle and magnitude relationships as the constraints. Besides, due to the periodicity in ω_l, we only consider the cases where the parameters in [α, $\boldsymbol{V}$] are greater than zero. $\mathbb{Z}^+$ denotes the set of nonnegative integer numbers. Through the optimization of Eq. (6), we can finally get optimal parameters [α, $\boldsymbol{V}$].

2) 4PSK→MPSK

In the WFRFT precoding scheme, through phase rotation, the WFRFT-disguising signals(4PSK) can be further transformed into MPSK. We only consider the condition that $M = 8$ and $M = 16$ because the analysis methods and related conclusions are similar for other conditions where $M = 2^{M_{ary}}(M_{\text{ary}} > 4)$.

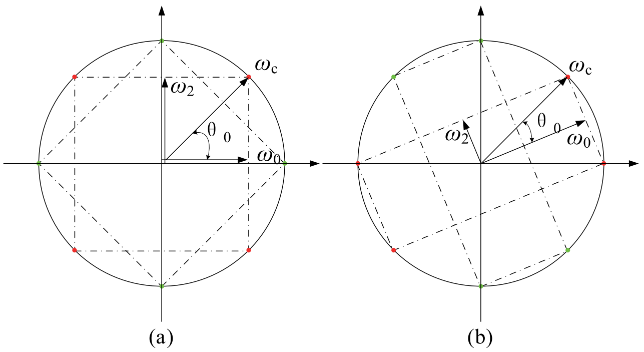

FIGURE 5. Rotation diagram for 4PSK→8PSK. (a) $\theta_0 = 4\pi/16$ (b) $\theta_0 = 2\pi/16$.

Fig. 5 illustrates two possible rotation patterns masking 4PSK into 8PSK. As for the basic four constellation points (red color points) of Fig. 5(a) and (b), by analyzing the basic geometry of Fig. 4, according to the definition of tangent function, the magnitude ratio of ω_2 to $\omega_0(|\omega_2|/|\omega_0|)$ correspond $\lambda = \tan(\theta_0)$.

As shown in Fig. 5(a) and Fig. 5(b), θ_0 has two possible values, namely, 22.5°($2\pi/16$) and 45°($4\pi/16$). Then, with one-bit mapping phase rotation, the finally 8PSK can be generated. Based on Fig. 5, the one-bit mapping matrix is listed in Table 1.

TABLE 1. One-bit phase mapping for 4PSK→8PSK.

Phase Mapping	0	1
$\lambda = \tan(4\pi/16\ )$	$0 * \pi/4$	$1 * \pi/4$
$\lambda = \tan(2\pi/16\ )$	$0 * \pi/4$	$2 * \pi/4$

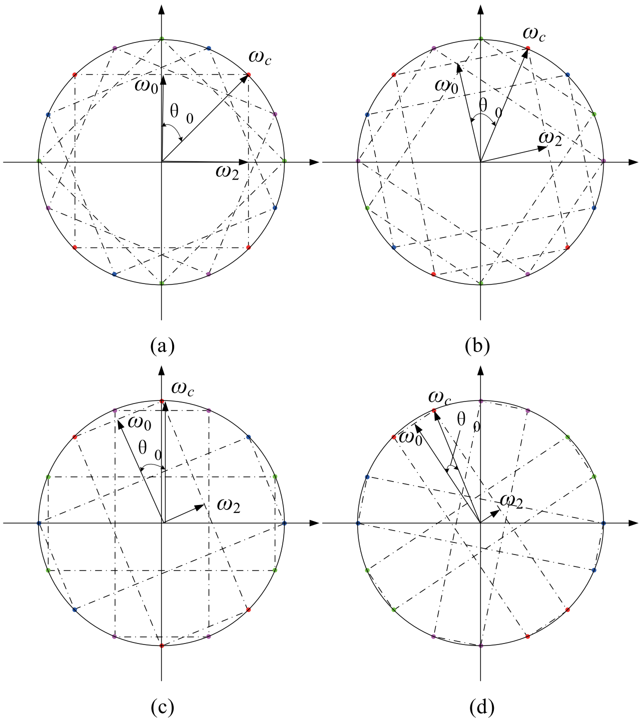

FIGURE 6. Rotation diagram for 4PSK→16PSK. (a) $\theta_0 = 4\pi/16$. (b) $\theta_0 = 3\pi/16$. (c) $\theta_0 = 2\pi/16$. (d) $\theta_0 = \pi/16$.

Fig. 6 illustrates four possible rotation patterns diagram masking 4PSK into 16PSK. With the same analysis method in Fig. 5 (4PSK→8PSK), we can get the four different conditions to mask 4PSK into 16PSK. Unlike one-step rotation Fig. 5 (4PSK→8PSK), there need four-step rotations in Fig. 6 (4PSK→16PSK).And the corresponding two-bit mapping matrix is listed in Table 2.

TABLE 2. Two-bit phase mapping for 4PSK→16PSK.

Phase Mapping	00	01	10	11
$\lambda = \tan(4\pi/16\ )$	$0 * \pi/8$	$1 * \pi/8$	$2 * \pi/8$	$3 * \pi/8$
$\lambda = \tan(3\pi/16\ )$	$0 * \pi/8$	$2 * \pi/8$	$4 * \pi/8$	$6 * \pi/8$
$\lambda = \tan(2\pi/16\ )$	$-3 * \pi/8$	$0 * \pi/8$	$1 * \pi/8$	$4 * \pi/8$
$\lambda = \tan(1\pi/16\ )$	$-2 * \pi/8$	$0 * \pi/8$	$2 * \pi/8$	$4 * \pi/8$

Through WFRFT precoding process in Fig. 6, the original signal $\boldsymbol{x}_0$ can be transformed into $\boldsymbol{S}$, in which the i-th element is S_i. Then, S_i can be simply regarded the quasi-8PSK or the quasi-16PSK signals. Thus, $\boldsymbol{S}\left(\boldsymbol{S} = [S_0, S_1, \cdots, S_{N-1}]^{\mathrm{T}}\right)$ is the vector form for the WFRFT precoding, which can be calculated by

$$\boldsymbol{S} = e^{-\mathrm{j}\boldsymbol{\vartheta}_{\mathrm{rot}}} \odot (\boldsymbol{W}_M^{\alpha,\boldsymbol{V}} \boldsymbol{x}_0) = \boldsymbol{p}_{\mathrm{rot}} \odot \boldsymbol{w} \tag{7}$$

where $\odot$ denotes the wise-product operation; $\boldsymbol{p}_{\mathrm{rot}}$ denote the rotating phase in the WFRFT process, and $\boldsymbol{p}_{\mathrm{rot}} = [p_{\mathrm{rot},0}, p_{\mathrm{rot},1}, \cdots, p_{\mathrm{rot},N-1}]^{\mathrm{T}}$. Besides, $p_{rot,i}, i = 0, 1, \cdots, N - 1$ are generated from the phase mapping Table 1 (4PSK→8PSK) or Table 2 (4PSK→16PSK). More details about the random phase $\boldsymbol{p}_{\mathrm{rot}}$ will be discussed in the next section.

C. DOUBLE-RANDOM PSEUDO PHASE GENERATION

As analyzed in the WFRFT Precod module of the former subsection, the original BPSK signals can be disguised into MPSK signals. Then the WFRFT precoding signals (MPSK) is embedded into the traditional TDCS. To enhance the communication's security, the random rotation phase in Table 1 and Table 2 are generated by the pseudo random number generator. In the frequency domain, the basic function (BF) phase vector $\mathrm{e}^{\mathrm{j}\boldsymbol{\vartheta}_{\mathrm{base}}}$ can be also generated by a m-sequence generator. In this subsection, we provide a double-random sequence generating scheme for BF's phase vector $\mathrm{e}^{\mathrm{j}\boldsymbol{\vartheta}_{\mathrm{base}}}$ in TDCS and rotation phase $e^{-\mathrm{j}\boldsymbol{\vartheta}_{\mathrm{rot}}}$ in WFRFT Precod module.

When $[\alpha, \boldsymbol{V}]$ in Eq. (3) is selected, the basic constellation distribution is totally decided. When the WFRFT and traditional TDCS with unchanged parameters in a long term, it's still unsafe because the unauthorized users can intercept the exchange information through the autocorrelation-based detection or feature extraction-based recognition methods [21]. So we should adopt other encrypting methods to further ensure the communication's security. Thus, a dynamically pseudo phase generation is proposed to assist enhancing the proposed system security. In [22], an effective method is provided to generate the pseudo phase based on m-sequences. According to [22], based on m-sequences, the proposed phase generation of this paper is operated as Fig. 7. For design's clarity, in our phase generation scheme, two parameter sets are utilized to

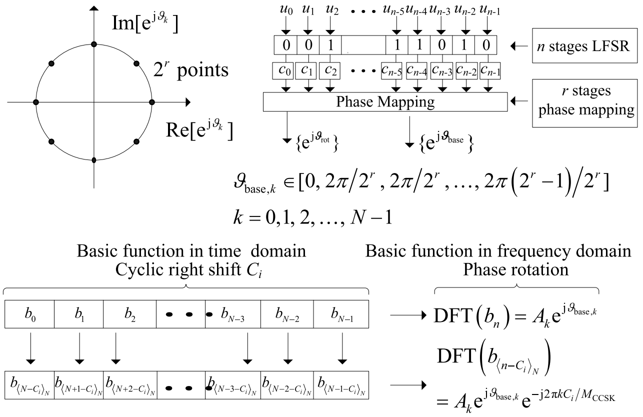
$\mathrm{Im}[\mathrm{e}^{\mathrm{j}\vartheta_k}]$
2^r points
$\mathrm{Re}[\mathrm{e}^{\mathrm{j}\vartheta_k}]$
u_0 u_1 u_2 • • • $u_{n\text{-}5}$ $u_{n\text{-}4}$ $u_{n\text{-}3}$ $u_{n\text{-}2}$ $u_{n\text{-}1}$
0 0 1 1 1 0 1 0
c_0 c_1 c_2 • • • $c_{n\text{-}5}$ $c_{n\text{-}4}$ $c_{n\text{-}3}$ $c_{n\text{-}2}$ $c_{n\text{-}1}$
n stages LFSR
Phase Mapping
r stages phase mapping
$\{\mathrm{e}^{\mathrm{j}\vartheta_{\mathrm{rot}}}\}$
$\{\mathrm{e}^{\mathrm{j}\vartheta_{\mathrm{base}}}\}$
$\vartheta_{\mathrm{base},k} \in [0, 2\pi/2^r, 2\pi/2^r, \ldots, 2\pi(2^r-1)/2^r]$
$k = 0, 1, 2, \ldots, N-1$
Basic function in time domain
Cyclic right shift C_i
Basic function in frequency domain
Phase rotation
b_0 b_1 b_2 • • • b_{N-3} b_{N-2} b_{N-1}
$b_{\langle N-C_i\rangle_N}$ $b_{\langle N+1-C_i\rangle_N}$ $b_{\langle N+2-C_i\rangle_N}$ • • • $b_{\langle N-3-C_i\rangle_N}$ $b_{\langle N-2-C_i\rangle_N}$ $b_{\langle N-1-C_i\rangle_N}$
$\mathrm{DFT}(b_n) = A_k \mathrm{e}^{\mathrm{j}\vartheta_{\mathrm{base},k}}$
$\mathrm{DFT}\left(b_{\langle n-C_i\rangle_N}\right)$
$= A_k \mathrm{e}^{\mathrm{j}\vartheta_{\mathrm{base},k}} \mathrm{e}^{-\mathrm{j}2\pi k C_i/M_{\mathrm{CCSK}}}$

FIGURE 7. Double-random sequence generator and Mapping process in TDCS.

dynamically generate the corresponding pseudo number, which can double guarantee the pseudo phases' security. And these two parameters are $[n, U_0]$, $U_0 = [u_0, u_1, \ldots, u_{n-1}]$ and $[r, C_0]$, $C_0 = [c_0, c_1, \ldots, c_{n-1}]$. There are three main steps to generate the BF pseudo phase in TDCS with CCSK baseband modulation:

Step 1: As for the basic function in TDCS, through liner feed shift register(LFSR), the first parameter set in $[n, U_0]$ is used to generate the m-sequences, which has a period of $2^n - 1$. $U_0 (U_0 = [u_0, u_1, \ldots, u_{n-1}])$ is the preset states for the LFSR, and U_0 can be set to all possible register states except the all-zeros state [23]. Different stages n and different initial states U_0 will generate different binary sequence $\boldsymbol{b} = [b_0, b_1, \cdots, b_{N-1}]^{\mathrm{T}}$ for the phase mapping module.

Step 2: With the binary sequence selection parameter set $[r, C_0]$, we choose the r LFSR outputs which usually include any combination of the n LFSR stages. The initial binary values $C_0 \left(C_0 = [c_0, c_1, \ldots, c_{n-1}]\right)$ is used to decide which r LFSR stages are selected, and C_0 satisfies the constraints $\sum_{i=0}^{n-1} c_i = r, r < n$. After double random process, the pseudo phase can $\vartheta_{\text{base},k}$, $k = 1, 2, \ldots, N$ belongs to the set $\{0,\ 2\pi/2^r\ 2\pi \cdot 2/2^r\ \ \ldots,\ 2\pi\left(2^r - 1\right)/2^r\}$. And $\boldsymbol{p}_0 = [p_{0,0}, p_{0,1}, \cdots, p_{0,N-1}]^{\mathrm{T}}$, $p_{0,k} = \mathrm{e}^{\mathrm{j}\vartheta_{\text{base},k}}$.

Step 3: As for CCSK modulation, in Fig. 5, for the basic function(BF) of TDCS, the corresponding mapping process from time domain to frequency domain is also depicted. According to the BF property: the cyclic shift in time domain corresponds the phase shifting in frequency domain [24]. The final BF phase $\boldsymbol{p}_{\text{base}}$ is generated from $\boldsymbol{p}_0$ after cyclic left shift C_i bits, namely, $p_{\text{base},k} = p_{0,k}\mathrm{e}^{-\mathrm{j}2\pi k C_i/M_{\text{CCSK}}} = \mathrm{e}^{\mathrm{j}\vartheta_{\text{base},k}}\mathrm{e}^{-\mathrm{j}2\pi k C_i/M_{\text{CCSK}}}$.

Then, as for the WFRFT rotation phase, to be consistent with the generation of $\boldsymbol{p}_0$, we can simply choose 1 or 2 bits out of the r LFSR outputs to generate the WFRFT rotation phase $\boldsymbol{\vartheta}_{\text{rot}}$, and $\boldsymbol{p}_{\text{rot}}$ in Eq.(7) can be calculated by $\boldsymbol{p}_{\text{rot}} = e^{-\mathrm{j}\boldsymbol{\vartheta}_{\text{rot}}}$.

D. RECEIVER

According to the embedding structure in Fig. 7, the final combinatory signal $\boldsymbol{X}$ can be expressed by

$$\boldsymbol{X} = \boldsymbol{S}\boldsymbol{B} \tag{8}$$

where $\boldsymbol{S}$ corresponds Eq.(7), and $\boldsymbol{S} = [\ S_0, S_1, \cdots, S_{N-1}\ ]^{\mathrm{T}}$; di$ag(\boldsymbol{S})$ returns a square diagonal matrix with vector $\boldsymbol{S}$ as the main diagonal; $\boldsymbol{B}$ is the BF matrix, whose (k, i)-th element is given by $B_{k,i} = A_k \mathrm{e}^{\mathrm{j}\vartheta_{\text{base},k}}\mathrm{e}^{-\mathrm{j}2\pi\cdot k\cdot C_i/M_{\text{CCSK}}}$.

Then, the (k, i)-th element of $\boldsymbol{X}$ in Eq.(8) can be calculated by

$$X_{k,i} = S_i B_{k,i} = A_k \mathrm{e}^{\mathrm{j}\vartheta_{\text{base},k}}\mathrm{e}^{-\frac{\mathrm{j}2\pi\cdot k\cdot C_i}{M_{\text{CCSK}}}} S_i \tag{9}$$

In Eq.(9), S_i can be simply regarded as a MPSK signal, then, without loss of generality, we can take the i-th row of $\boldsymbol{X}$ as an example to analyze the system's recovery performances. At Tx, the WFRFT-TDCS combinatory signal $\boldsymbol{x}$ can be expressed by

$$\boldsymbol{x} = \left[X_{0,i}, X_{1,i}, \cdots, X_{N-1,i}\right]^{\mathrm{T}} \tag{10}$$

Then, at Tx, the final transmitting signal $\boldsymbol{t}$ is expressed by

$$\boldsymbol{t} = \boldsymbol{F}_N^{-1}\boldsymbol{x} \tag{11}$$

Over AWGN channel, at Rx, through OFDM demodulated module, $\boldsymbol{x}$ can be transformed into

$$\boldsymbol{y} = \boldsymbol{F}_N(\boldsymbol{t}+\boldsymbol{n}) = \boldsymbol{x} + \boldsymbol{n}' \tag{12}$$

In Eq.(12), $\boldsymbol{n}$ is the AWGN noise vector, and $\boldsymbol{n} = [n_0, n_1, \cdots, n_{N-1}]^{\mathrm{T}}$. For sake of clarity, we use the short notation $n_k \sim N(\mu,\sigma^2)$ to describe the properties of Gaussian distributed random variable, where μ and σ^2 are the expected value and the variance of n_k respectively. Then, considering the DFT matrix $\boldsymbol{F}_N$ is a unitary linear transformation, $\boldsymbol{n}'(\boldsymbol{n}' = \boldsymbol{F}_N\boldsymbol{n})$ will obey the same statistical distribution property, that is, is $n'_k \sim N(\mu,\sigma^2)$, and n'_k is the k-th element of $\boldsymbol{n}'$.

As shown in Fig. 3, to recover the original data, we should take the following two steps: 1) CCSK Demod; 2) WFRFT Decod. Besides, because the WFRFT Decod process relies on the recovery performance of BF at Rx, we will conduct the process of CCSK Demod prior to WFRFT Decod. Fig. 8 depicts the combinatory recovery scheme for CCSK Demod and WFRFT Decod. More details about the combinatory recovery will be analyzed in the following two subsections.

1) CCSK DEMOD

As for the CCSK Demod process, according to periodic convolution theorem, the DFT of the product of two discrete sequences is the periodic convolution of the DFTs of the individual sequence [25]. Let $\boldsymbol{u}$, $\boldsymbol{b}$ and $\boldsymbol{g}$ be the time domain signal of input, basic function and output in vector form respectively. Then, the following formula can be utilized as an efficient way to recover the original input signal

$$\begin{aligned} \boldsymbol{g} &= \left\{\mathrm{IDFT}\left\{\mathrm{DFT}\left\{\boldsymbol{u}\right\}\left(\mathrm{DFT}\left\{\boldsymbol{b}\right\}\right)^*\right\}\right\} \\ &= \boldsymbol{F}_N^{-1}\left[\boldsymbol{F}_N(\boldsymbol{u})(\boldsymbol{F}_N(\boldsymbol{b}))^*\right] \end{aligned} \tag{13}$$

where $(\cdot)^*$ denotes conjugate calculation.

Owing to the fact that only the real parts of the received signal will finally make a sense on the recovery of the original transmitting signal, we can conduct the final CCSK Demodulation as follows

$$\boldsymbol{g} = \mathrm{Re}\left\{\boldsymbol{F}_N^{-1}\left[\boldsymbol{F}_N(\boldsymbol{u})(\boldsymbol{F}_N(\boldsymbol{b}))^*\right]\right\} \tag{14}$$

where $\mathrm{Re}(\cdot)$ denotes the function to get the real part of a complex number.

In this paper, we assume that the amplitude of basic function in Tx and Rx are the same, that is, $A_k = A'_k$. Then, as depicted in Fig. 8, $\mathrm{DFT}\left\{\boldsymbol{u}\right\} = \boldsymbol{y}$, $\mathrm{DFT}^*\left\{\boldsymbol{b}\right\} = [A_0\mathrm{e}^{-\mathrm{j}\vartheta_{\text{base},0}}, A_1\mathrm{e}^{-\mathrm{j}\vartheta_{\text{base},1}}, \cdots, A_{N-1}\mathrm{e}^{-\mathrm{j}\vartheta_{\text{base},N-1}}]^{\mathrm{T}}$.

Let $\boldsymbol{v} = [v_0, v_1, \cdots, v_{N-1}]^{\mathrm{T}}$, then the k-th element $v_k = y_k A_k \mathrm{e}^{\text{-}\mathrm{j}\vartheta_{\text{base},k}}$. The index of maximum $\boldsymbol{g}$ can be used as the estimated value of C_i. Then the estimated CCSK demodulated signal, $\hat{C}_i$ can be obtained as follows

$$\hat{C}_i = \arg\max_k\ (\boldsymbol{g}) = \arg\max_k\ \left(\mathrm{Re}\left\{\mathrm{IDFT}\left\{\boldsymbol{v}\right\}\right\}\right) \tag{15}$$

When $M_{\text{CCSK}} = N$, $\hat{C}_i$ can be calculated directly by Eq.(15). When $M_{\text{CCSK}} < N$, a weighting coefficient $\beta = M_{\text{CCSK}}/N$ should be added to adjust the exact $\hat{C}_i$ based on Eq.(15), and then the modified estimated signal $\hat{C}_i$ can be calculated by

$$\hat{C}_i = \left\lfloor \beta \hat{C}' + 0.5 \right\rfloor = \left\lfloor (M_{\text{CCSK}}/N)\hat{C}' + 0.5 \right\rfloor \tag{16}$$

where $\hat{C}'$ is the initial value calculated by Eq.(15), and $\lfloor\cdot\rfloor$ denotes the function to get the nearest integer less than or equal to the original number.

2) WFRFT DECOD

As illustrated in Fig. 3, after CCSK Demod, the estimated signal $\hat{C}_i$ would further be used to revise the phase shift $e^{-j2\pi\cdot k\cdot C_i/M_{\text{CCSK}}}$ for the original BF. According to the WFRFT Decod process in Fig. 8, combining with the frequency-domain BF vector $A_k e^{j\vartheta_{\text{base},k}}$ and the rotation phase $e^{j\vartheta_{\text{rot},i}}$, we can estimate the final $\hat{S}_i$ as follows

$$\hat{S}_i = \frac{1}{N}\sum_{k=0}^{N-1}\left\{ y_k \left(A_k e^{j\vartheta_{\text{base},\,k}} e^{-j\theta_{\text{rot},\,i}} e^{\frac{-j2\pi \hat{C}_i k}{M_{\text{CCSK}}}} \right)^* \right\} \tag{17}$$

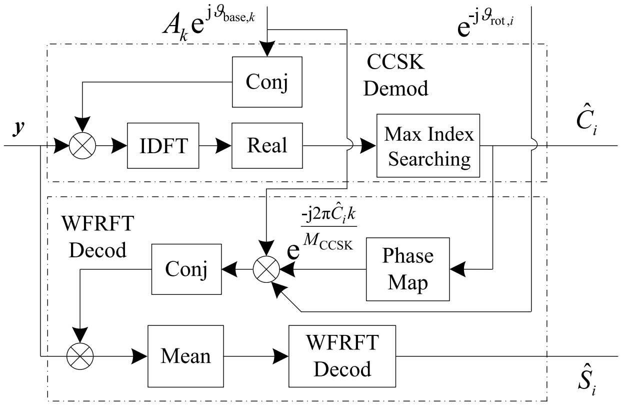

FIGURE 8. Combinatory Recovery scheme for CCSK and WFRFT.

Then, through $(-\alpha)$ order WFRFT, we can recover the signal as follows

$$\hat{\boldsymbol{x}}_0 = \boldsymbol{W}_4^{-\alpha,\boldsymbol{V}}\hat{\boldsymbol{s}} \tag{18}$$

where $\hat{\boldsymbol{s}} = [\,\hat{S}_0, \hat{S}_1, \cdots, \hat{S}_{N-1}\,]^{\text{T}}$, and $\boldsymbol{W}_4^{-\alpha,\boldsymbol{V}}$ corresponds Eq.(3).

IV. THEORETICAL PERFORMANCES

A. POWER SPECTRAL DENSITY

According to [26], when utilizing embedded symbols in the CCSK-based TDCS system, the power spectral density (PSD) can be calculated by

$$\text{PSD}(f) = \frac{1}{N}\left| A_{\text{P}} e^{j\varphi_{\text{P}}} \sum_{k=0}^{N-1} A_k e^{j\vartheta_{\text{base},k}} \int_{-\frac{T(1+\gamma)}{2}}^{\frac{T(1+\gamma)}{2}} p(t) e^{-j2\pi(f-f_k)t} \text{d}t \right|^2 \tag{19}$$

where A_{P} and φ_{P} are the magnitude and phase of the embedded symbol respectively, T is the signal's duration; $p(t)$ is the window function, γ is the corresponding roll-off factor of the window. Based on Eq.(19), as PSK symbols are distributed on a unit circle, embedding PSK symbols into TDCS-CCSK will not enlarge the sidelobes. Considering the WFRFT precoding signals behave like the quasi-MPSK symbols. Then, as for the WFRFT-TDCS combinatory system in Fig. 3, the embedded WFRFT precoding symbols wouldn't bring a severe damage on the traditional TDCS performance.

B. SPECTRAL EFFICIENCY

According to the analyses in subsection 3.4.2 (WFRFT Precod), for one TDCS symbol transmission, another one 2PSK symbol is embedded into TDCS, while causing no effect on the system's bandwidth, Then, we can derive that the spectrum efficiency η for the designed TDCS with WFRFT precoding symbols embedded system can be given by

$$\eta = \log_2(2\cdot M_{\text{CCSK}})/N(\text{b/s/Hz}) \tag{20}$$

According to Eq.(20), with the same spreading factor, N, the spectrum efficiency of the proposed system in this paper can gain $\log_2(M_{\text{CCSK}})/N$ more than the ones of the traditional direct sequence spread spectrum (DS-SS) and hybrid carrier code division multiple access (HC-CDMA) systems. Compared to the traditional TDCS, there exists another $\log_2(2)/N = 1/N$ gain in the proposed system of this paper.

C. ANTI-AWGN CAPABILITY

In the proposed system, as for CCSK Demod, the interferences mainly come from $\boldsymbol{n}'$ in Eq.(12). And $\boldsymbol{n}' = \boldsymbol{F}_N\boldsymbol{n}$. Owing to the unitary property of DFT matrix $\boldsymbol{F}_N$, $\boldsymbol{n}'$ obeys the same Gaussian distribution with the original noise $\boldsymbol{n}$.

As for WFRFT Decod, according to Eq.(8), the BF vector $A_k e^{-j\vartheta_{\text{base},k}}$ can be regarded as an spread sequence to some extent, the equivalent signal-noise ratio can be calculated by

$$\text{SNR} = (\log_2(M_{\text{PSK}})/N)\cdot E_{\text{b}}/N_0 = 1/N\cdot E_{\text{b}}/N_0 \tag{21}$$

Based on Eq.(21), we can conclude that WFRFT precoding process can gain $\log_2(N)$ dB compared with the traditional baseband modulation scheme.

D. ANTI-EAVESDROPPING CAPABILITY

In Fig. 3, the WFRFT Precoding parameter set $[\alpha, \boldsymbol{V}]$ and double-random pseudo phase generation scheme are unknown to the unauthorized receivers. Because WFRFT-based system has a strong anti-parameter scanning ability [27], [28], it becomes difficult for the unauthorized receivers to eavesdrop the current WFRFT parameter set $[\alpha, \boldsymbol{V}]$ timely. Besides, the double-random scheme in DRP Gen of Fig. 3 can generate the expected pseudo number, and then generate the corresponding pseudo phase. The different parameter sets selections($[n, U_0]$ and $[r, C_0]$) can protect the system from being intercepted through the autocorrelation-based or statistic-based detection methods, and further guarantee the communication system's security.

V. NUMERICAL SIMULATIONS

In this section, to examine the combined TDCS with WFRFT for secure transmission, we conduct the following numerical simulations over AWGN channels with block length of $N = 512$. To reduce the computational complexity, the FFT algorithm is used to implement the DFT module of Fig. 1 in the simulation.

A. WFRFT PRECODING CONSTELLATIONS

1) CONSTELLATIONS FOR 2PSK→4PSK

We first test the constellation disguising property in the WFRFT Precod module in Fig. 4. Through WFRFT processing, the original BPSK baseband signal can be disguised into 4PSK. Considering that genetic algorithm(GA) can converge to the global minima in a probability of 90% [29]–[31], we adopt GA to solve the optimization program in Eq.(6), and initial searching conditions are Generations $=$ 100, PopulationSize $=$ 20, CrossoverFraction $=$ 0.8, and ParetoFraction $=$ 0.35. The related bounds in Eq.(6) are $A = 4$, $Q = 100$. To test the constellation properties caused WFRFT precoding process, as for the optimization program in Eq(6), for analyses' clarity, we let $\delta_2 = \lambda\delta_1$. Besides, according to the unitary transformation property, we can obtain $|\omega_0|^2 + |\omega_1|^2 + |\omega_2|^2 + |\omega_3|^2 = 1$ [32]. Therefore, we can select the quasi-Gaussian constraint δ_3 as follows: $\delta_3 = 0.5[1 - (1 + \lambda^2)(\delta_1)^2]$. Then we just pay our attention to the following constraints, δ_1 and λ. In the following simulations, to make the time domain signals($\omega_0\boldsymbol{x}_0 + \omega_2\boldsymbol{x}_2$) be the predominant one in Eq.(5), we further let $\delta_1 = 0.999/(1 + \lambda^2)$. According to magnitude ration relationship in Table 1 and Table 2, the ratio constraint λ could be set to following four possible values: $\tan(\pi/16)$, $\tan(2\pi/16)$, $\tan(3\pi/16)$, and $\tan(4\pi/16)$. Then we can get the corresponding four values for δ_1: 0.9798, 0.9230, 0.8306, and 0.7064. Through GA, we can obtain the corresponding parameter set $[\alpha, \boldsymbol{V}]$, which are shown in the paras iii-v of Table 3 respectively.

TABLE 3. Parameters $[\alpha, V]$ in different WFRFT precoding patterns.

Paras	i	ii	iii	iv	v
α	2.4567 8472	0.7328 4959	1.1554 2485	2.9371 8068	2.7689 2907
$\boldsymbol{MV}$	[54 85 58 46]	[0 40 43 43]	[50 69 17 54]	[5 62 84 75]	[42 59 43 22]
$\boldsymbol{NV}$	[85 84 41 40]	[61 32 40 32]	[30 11 64 64]	[68 87 33 32]	[37 50 65 53]
$\langle\omega_0\rangle$	-144.3335	-27.4095	144.7762	51.5427	-3.0503
$\langle\omega_0, \omega_2\rangle$	25.4079	-90.0193	-89.9974	89.9951	90.0064
λ	0.8628	0.2131	0.4174	0.6844	0.9992
$\lvert\omega_1\rvert + \lvert\omega_3\rvert$	0.9989	0.0003	0.0004	0.0006	0.0003

Moreover, to clearly exhibit MP-WFRFT signals' Gaussian-like characteristic, we also revise the magnitude constraints to $\max(|\omega_1|, |\omega_3|) > \delta_3$, and $\delta_3 = 0.5$ in Eq. (6),and the paras i of Table 3 corresponds the parameter set $[\alpha, \boldsymbol{V}]$ and its related operation results. According to the values of $|\omega_1| + |\omega_3|$ in Table 3, we can conclude that the quasi-Gaussian noise's power is directly controlled by the magnitude sums of ω_1 and ω_3. The larger $|\omega_1| + |\omega_3|$ is, the stronger the quasi-Gaussian characteristic gets.

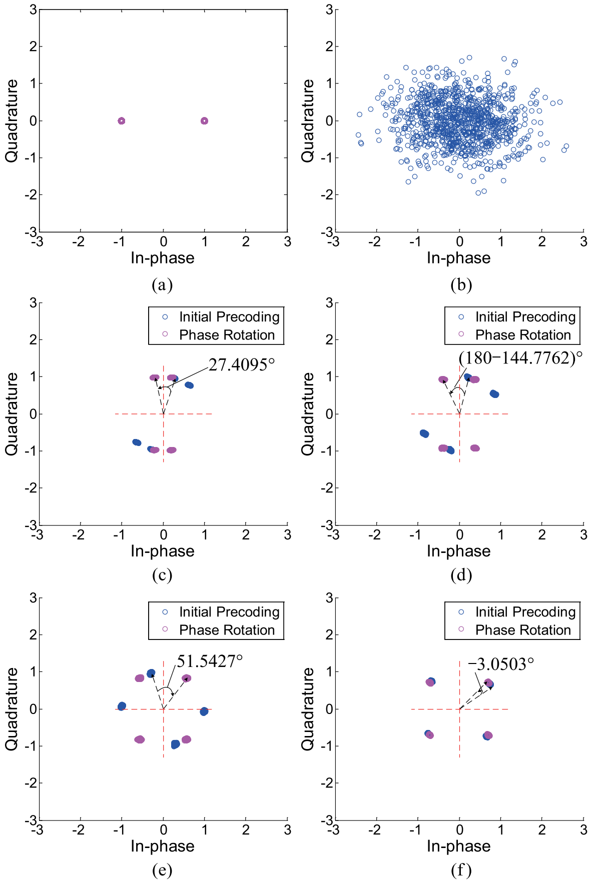

(a)

(b)

(c)

(d)

(e)

(f)

FIGURE 9. Constellations disguising 2PSK into 4PSK with WFRFT precoding and phase rotation. (a) Original BPSK. (b) WFRFT Precod with Paras I. (c) WFRFT Precod with Paras ii. (d) WFRFT Precod with Paras iii. (e) WFRFT Precod with Paras iv. (f) WFRFT Precod with Paras v.

To observe the constellation disguising more clearly, we also plot the corresponding WFRFT-processing constellations based on Table 3, which are shown in Fig. 9. Fig. 9(a) corresponds the basic constellations of 2PSK. Fig. 9 (b)-(f) corresponds different patterns i-v in Table 3 respectively. In Fig. 9(b)-(f), through the phase rotation, WFRFT precoding constellatons (blue points) can be further revised into the standard constellations (purple points) that are symmetrical to X-Y axes.

2) CONSTELLATIONS FOR 4PSK→8/16PSK

To further encrypt the original BPSK constellation, the WFRFT-processing constellations of Fig. 9 can be disguised into Mary-PSK(MPSK) through the randomly rotating processing of Fig. 9. As for the randomly rotating processing, the pseudo sequence with its corresponding mapping phase are listed in Table 1 and Table 2.

As shown in Fig. 10, when we choose the parameter set v in Table 3, through phase rotation, we can get the initial

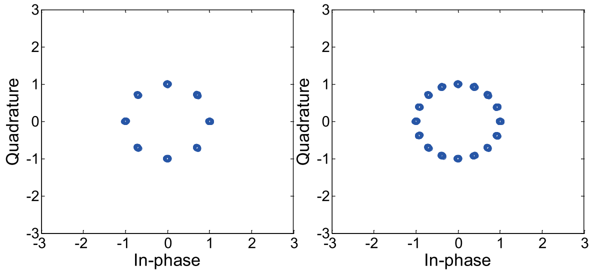

(a) (b)

FIGURE 10. Constellations disguising 4PSK into 8/16PSK with random phase rotation.

WFRFT precoding constellations (shown in Fig. 9(f)). Moreover, the WFRFT precoding constellations can be further disguised into 8PSK with one-bit random phase mapping (the case where $\lambda = \tan(4\pi/16)$ in Table 1), and can be also disguised into 16PSK with two-bit random phase mapping (the case where $\lambda = \tan(4\pi/16)$ in Table 2). The constellation disguising law is quite consistent with the one in Fig. 5(a) and Fig. 6(a).

B. BIT ERROR RATE PERFORMANCE FOR AUTHORIZED RECEIVERS

As demonstrated in the constellation disguising analysis of the former subsection, the WFRFT precoding method in Fig. 9 and Fig. 10 can double guarantee the communication security of the original embedded BPSK signal. To further test the BER performance of proposed system for the authorized transmissions in Fig. 3, representative results are averaged over 1000 trials to improve the simulation's accuracy.

We select the mapping phase where $\lambda = \tan(4\pi/16)$ in Table 1 and Para v is adopted in Table 3 to disguise the original BPSK constellation. Based on the double pseudo-random number generator in Fig. 7, as for the two parameter sets $[n, U_0]$, $[r, C_0]$ in the double-random phase generation of Fig. 7, we set $n = 12$, $r = 10$, and U_0, C_0 are set randomly. In addition, signal to noise ratio(SNR) is set in $[-25, -13]$ dB, with precision 2dB.

According to the theoretical analyses in Fig. 8, the original embedded BPSK signals' bit error rate (BER) performances rely on the correctness of CCSK symbol's demodulation. Thus, we test the CCSK SER performances and the embedded BPSK BER performances with different M_{CCSK}. As depicted in Fig. 11, with the increase of M_{CCSK}, there is a slight decrease for CCSK symbol error rate (SER) performances correspondingly. However, due to the spreading gain N of TDCS BF sequence, the BPSK BER performances' differences become obvious with different M_{CCSK}. When M_{CCSK} gets smaller, the corresponding system's performances can be improved at the cost of spectral efficiency, which is consistent with Eq.(18).

Moreover, we also conducted the related simulations to test how WFRFT can affect the traditional TDCS system's performance on narrow band interference (NBI) suppression.

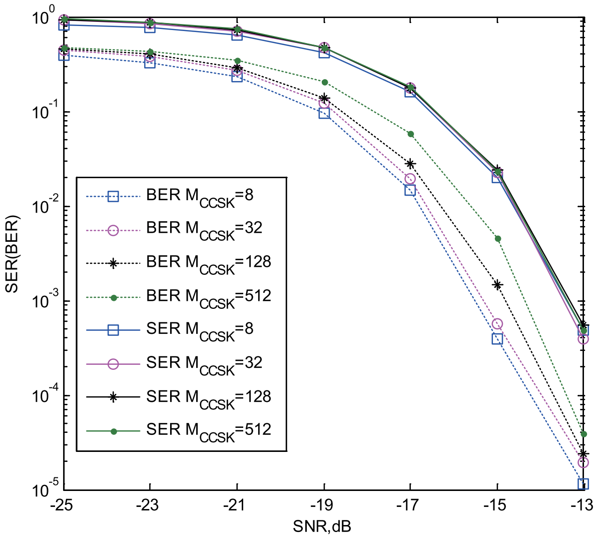

FIGURE 11. BER performances for authorized receivers with different M_{CCSK}.

As for the Fourier-based TDCS, we assume the NBI signal is stationary. According to [33], the basic model is built as follows

$$i_n = \sum_{k=0}^{K-1} g_k \exp[j(\frac{2\pi f_0(n-kT)}{N} + \varphi)], \quad n = 0, 1, \cdots, N-1 \tag{22}$$

where T is the period of each data symbol, K is bandwidth ratio of wideband system to NBI, and $K = \lceil N/T \rceil$, and $\lceil A \rceil$ means to round the elements of A to the nearest integers greater than or equal to A; f_0 denotes the central frequency of NBI, and g_k denotes the k-th data symbol.

And as for NBI in Eq.(22), the spreading factor K is set to 32, and the central frequency f_0 is set to 0.5 normalized block length. g_k obeys Bernoulli distribution, and the initial phase φ is uniformly distributed in $[0, 2\pi]$. As for the Threshold Decision model in Fig. 2 (Architecture of the WFRFT-TDCS combinatory system), the threshold for TDCS λ_{thre} is set to $0.4J_{\max}$, and $J_{\max}$ is the maximum spectrum amplitude for NBI, that is, for the i-th frequency, when NBI's amplitude $J_i > \lambda_{\text{thre}}$, the corresponding BF's amplitude A_i is set to 0, then the strong interference in i-th frequency can be eliminated. When NBI's amplitude $J_i < \lambda_{\text{thre}}$, the corresponding BF's amplitude A_i NBI is set to 1. And the power ratio of NBI to transmitting signal is defined as JSR, which is set in the range $[-10, 0]$dB. As for AWGN, SNR is still set in the range $[-25, -3]$dB.

Besides, in order to enhance the comparability between WFRFT-TDCS system and the traditional TDCS system, we simply replace the 'WFRFT Precod' and 'WFRFT Decod' modules with '4PSK Mod' and '4PSK Demod' modules, and test the CCSK SER performance for each system. Under the same channel states with NBI and AWGN, the simulations

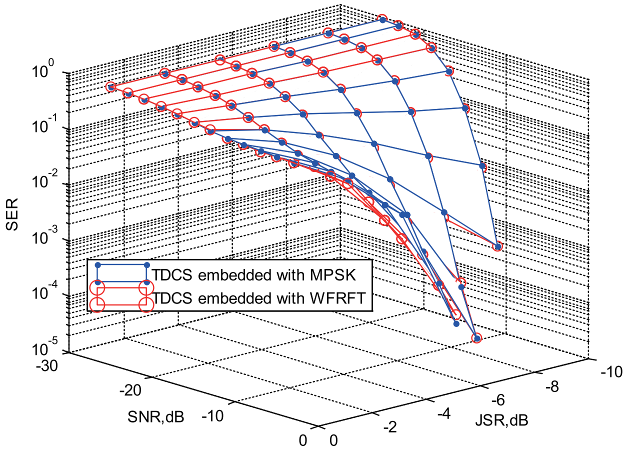

FIGURE 12. Anti-NBI capacity with different TDCS embedded structure.

are conducted and the CCSK SER performance comparisons are illustrated in Fig. 12.

As shown in Fig. 12, the CCSK performance in the traditional TDCS system are slightly better than the one in the WFRFT-TDCS system. The reason for the slight performance differences can be explained as follows:

As can be observed in Fig. 9(f), the WFRFT precod constellation are almost the same with the standard 4PSK constellation, which finally demonstrates that the quasi-4PSK can be obtained through WFRFT precod module. As analyzed in Eq.(19), PSK symbols are distributed on a unit circle, and embedding PSK symbols into CCSK-based TDCS will no enlarge the sidelobes, then won't affect the CCSK performance of TDCS. The slight constellation difference between the quasi-4PSK in WFRFT Precod module and the standard 4PSK will cause a slight PSD deviation, then further cause a slight CCSK SER performance degradation in WFRFT-TDCS system. However, the slight difference can be neglected especially when JSR > -8 dB and SNR < -15dB. Thus we can draw the conclusion that WFRFT will cause a slight affect on the original CCSK Demodulation performance and can be well compatible with the traditional TDCS system.

In Fig. 12, when we set JSR= − 10dB, with SNR varying in $\{-17, -15, -13\}$dB, the corresponding SER are $8 \times 10^{-3}, 7 \times 10^{-2}, 2.6 \times 10^{-1}$ respectively. While for the WFRFT-TDCS system without NBI, with the same SNR selections, the corresponding SER are $5 \times 10^{-3}, 2.3 \times 10^{-2}, 1.8 \times 10^{-1}$ respectively, as can be observed in Fig. 11. There exists an obvious performance degradation between the WFRFT-TDCS system with NBI and the one without NBI, which can be attributed to the basic function (BF) sequence's autocorrelation deduction and residual NBI interference.

C. SECURE PERFORMANCES

Based on the three steps of eavesdropping process in the earliest stages of the system description, according to [34], the system's security can be fully evaluated from the following three aspects: Low Probability of Detection(LPD), Low Probability of Interception(LPI), Low Probability of Exploration(LPE).

1) LOW PROBABILITY OF DETECTION

In order to evaluate the combinatory system's Low Probability of Detection (LPD) property, as the transmitting signals behave like the CCSK-based TDCS signals, we mainly pay our attention to the TDCS signals' LPD property. To focus on the TDCS signal, we simply substitute WFRFT precod with the MPSK Modulations. The basic MPSK modulation types and its corresponding size are assumed to be known to the unauthorized users. Then the correlation-detection method is adopted [35]. With a proper threshold, the correlation value between the original MPSK signals and the receiving signals can be used to decide whether the transmission is present or not. For comparison, we also exhibit the LPD performance for the PN(Pseudo Number)-based system. And the final LPD performances are illustrated in Fig. 13.

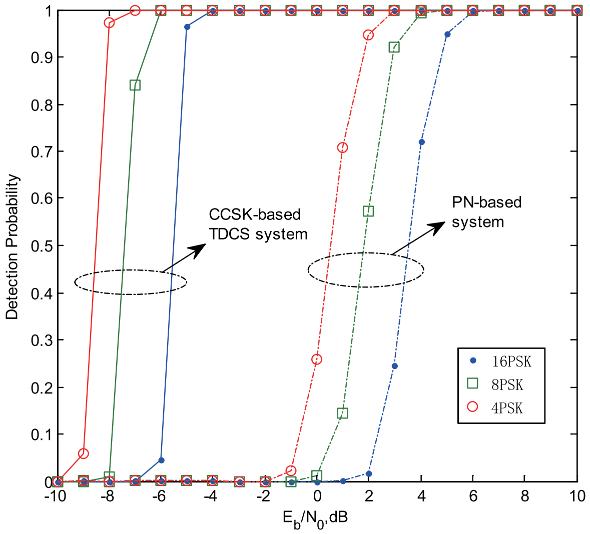

FIGURE 13. Detection performance comparison for PN-based and TDCS-based system.

In the view of the fact that the different baseband orders will affect the corresponding SNR(shown in Eq.(21)), we conduct the related simulations under the same E_b/N_0 and E_b/N_0 is set in the range $[-10, 10]$dB. As can be observed, with the increase of the MPSK baseband orders, the detection rate has a corresponding decrease. This is mainly because when the MPSK baseband orders get larger, the constellation points will distributed more uniformly on a unit circle, which will reduce the correlation value between the original MPSK signals and the receiving signals and then degrade the detection performance under the same AWGN channel states. When comparing the LPD performance between PN-based system and TDCS system, there exists almost a difference 8dB when detection probability is equal to 0. Although TDCS-based signals have almost the same pseudo generation scheme with PN-based signals, the CCSK modulation in

TDCS can scramble the original pseudo periodicity and then protect the transmitting signal from being detected by other unauthorized users.

2) LOW PROBABILITY OF INTERCEPTION

In the WFRFT Procod scheme of Fig. 3, the WFRFT processing signals are embedded into the traditional TDCS. Through WFRFT processing, the original BPSK signals can be disguised into MPSK and can help reduce the recognition probability by other eavesdroppers In addition, as shown in Fig. 7, the double pseudo-random sequence generation mechanism can further protect the legitimate transmitting signals from being captured. Thus, through the WFRFT processing and double pseudo-random sequence, the proposed system's communication's security can be guaranteed.

To analyze the proposed system's performance more precisely, we define the comprehensive BER (CBER) as follows

$$\text{CBER} = \text{BER}_\text{B} \cdot \frac{1}{1+\log_2(M_\text{CCSK})} + \text{BER}_\text{C} \cdot \frac{\log_2(M_\text{CCSK})}{1+\log_2(M_\text{CCSK})} \tag{23}$$

where BER_B and BER_C denote the BER performances of BPSK and CCSK modulations respectively.

In the following two simulations about the system's communication security, the CBERs are tested and illustrated to demonstrate the proposed systems' performance. We also select $M_\text{CCSK} = 512$ for sake of clarity.

According to whether the unauthorized users intercepted the WFRFT modulation modes or not, we can analyze the Low Probability of Interception(LPI) property for the combinatory system. The WFRFT precod has different splitting patterns and phase rotation schemes (shown in Fig. 9), so we pay our attention to the anti-scanning performance of WFRFT processing embedded signals to evaluate the combinatory system's LPI property.

The anti-scanning performance of WFRFT processing embedded signals is demonstrated with regards to BER. The channel is assumed to be only influenced by AWGN. Fig. 14 shows the BER comparisons between authorized receiver and eavesdropper. When the WFRFT precoding information (the WFRFT process and related rotation mapping information) is unknown to the eavesdropper, the original BPSK is disguised into Mary-PSK and totally cannot be recovered by the eavesdropper. Then as for Eq.(23), BER_B can be almost equal to 1, which also explain why there exists an error floor at CBER $= 10^{-1}$ even though SNR is getting large enough, as depicted in Fig. 14(i). When WFRFT precoding information is totally known to the eavesdropper, and the parameter scanning method is adopted to intercept the WFRFT parameters $[\alpha, \boldsymbol{V}]$. Fig. 14(ii)-(iv) illustrate the CBER compassions under different scanning error conditions. As can be observed in Fig. 14(ii)-(iv), even a subtle scanning error, i.e. $\Delta n = 1$, $\Delta m = 1$ and $\Delta\alpha = 0.001$, can still yield great CBER performance deterioration, which means that it's quite difficult for the eavesdropper to demodulate the original BPSK signals by scanning WFRFT parameters $[\alpha, \boldsymbol{V}]$. Especially, when the authorized system select its WFRFT precod modes and parameters $[\alpha, \boldsymbol{V}]$ in a cycle time less than the time needed in the scanning process, it's impossible for the unauthorized users to intercept the correct modes and parameters by scanning methods, and then the LPI property can be guaranteed.

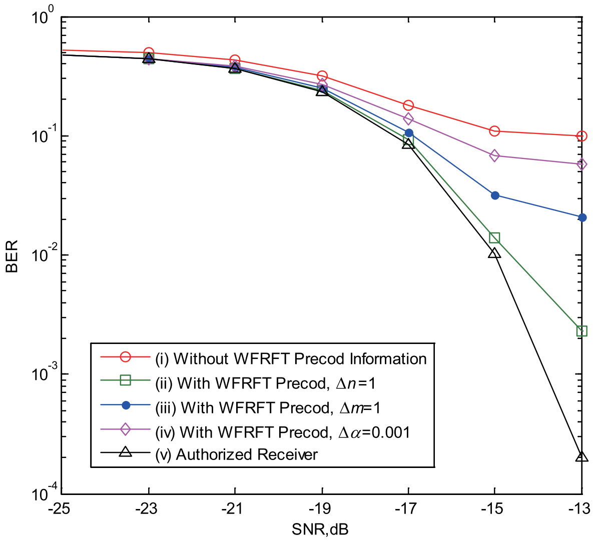

FIGURE 14. Anti-parameter scanning abilities for different parameter offset.

3) LOW PROBABILITY OF EXPLOITATION

After the unauthorized users has detected the presence of the transmission and also known the WFRFT Precod modes and TDCS's pseudo sequence, the only difference between authorized users and unauthorized users is that the dynamic selection of the parameter set $[\alpha, \boldsymbol{V}]$. As for the unauthorized users, the parameter error will inevitably affect the system's BER performances.

To further evaluate the built-in security enhancement property of the proposed system, with the same prior information of the authorized system, we compare the secrecy performance of the proposed system with the one of the HC-CDMA and PN systems. The simulation results are shown in Fig. 15. As for the direct sequence spread spectrum (DSSS) or the traditional TDCS, according to intrinsic periodicity of the pseudo-random sequences, time domain delay correlation algorithm [21] can be employed to acquire the period of the pseudo-random sequence and further to recover the corresponding pseudo-random sequence. As shown in Eq.(3), WFRFT-TDCS and HC-CDMA can both achieve better secrecy performance than the tradition DSSS, mainly because the WFRFT processing with different α will destroy the sequence correlation and then deteriorate demodulation BER performance). In addition, there is only one parameter WFRFT order α in HC-CDMA, unlike HC-CDMA, the parameters in WFRFT-TDCS are 9 (1 real number α and 8 integer of $\boldsymbol{V}$). The multiplicity of WFRFT parameters

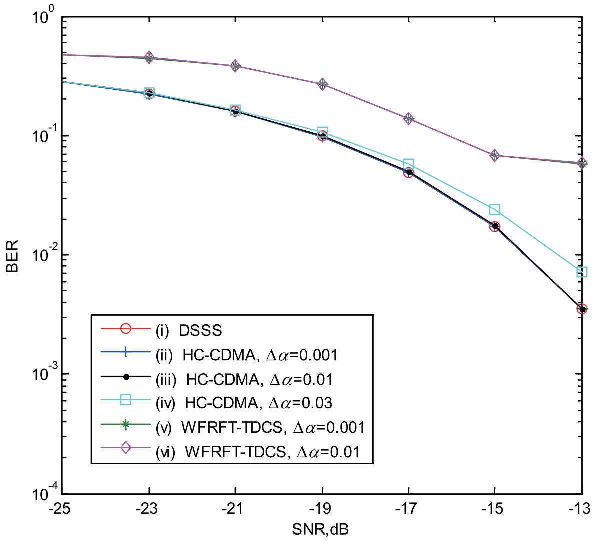

FIGURE 15. Anti-eavesdropping capacity for different communication systems.

($[\alpha, \boldsymbol{V}]$) will bring about a large amount of constellation splitting patterns (as shown in Fig. 9), and then make the proposed system's performance more sensitive to the parameter deviations, which can finally guarantee the better secrecy performance compared with HC-CDMA. Then we can draw the conclusion that the proposed WFRFT-TDCS system can has a lower probability of exploitation than the HC-CDMA and traditional DSSS system.

VI. CONCLUSION

In this paper, we propose a novel combinatory WFRFT-TDCS strategy to enhance the communication security. By embedding WFRFT precoding signals into the traditional TDCS system, the system's spectral efficiency can be enhanced while the corresponding communication quality is less impacted. The WFRFT precoding method can disguise the original signal into other higher order baseband modulations, and then further protect the system from being intercepted by other unauthorized users. Besides, the double-random phase generation scheme is designed to guarantee the combinatory WFRFT-TDCS system's communication security. Final simulations demonstrate that the proposed combinatory WFRFT-TDCS system can gain better anti-eavesdropping capacity while maintaining its own communication quality. To testify the proposed system's practicability, future works will focus on the performance of more different channels, such as narrow band interference, and multipath fading channels. Moreover, considering Fourier-based TDCS is often applied to the stationary interference, the improved Wavelet-based WDCS(wavelet domain communication system) will also be combined with WFRFT in our future work to enhance the system's anti-interference ability.

ACKNOWLEDGMENT

The authors would like to thank the anonymous referees for their great constructive comments to improve our work.

REFERENCES

[1] E. Onggosanusi *et al.*, "Modular and high-resolution channel state information and beam management for 5G new radio," *IEEE Commun. Mag.*, vol. 56, no. 3, pp. 48–55, Mar. 2018.

[2] Y. Cai, Z. Qin, F. Cui, G. Y. Li, and J. A. McCann, "Modulation and multiple access for 5G networks," *IEEE Commun. Surveys Tuts.*, vol. 20, no. 1, pp. 629–646, 1st Quart., 2018.

[3] S. Bayat, R. H. Y. Louie, Z. Han, B. Vucetic, and Y. Li, "Physical-layer security in distributed wireless networks using matching theory," *IEEE Trans. Inf. Forensics Security*, vol. 8, no. 5, pp. 717–732, May 2013.

[4] L. Xiao, X. Wan, and Z. Han, "PHY-layer authentication with multiple landmarks with reduced overhead," *IEEE Trans. Wireless Commun.*, vol. 17, no. 3, pp. 1676–1687, Mar. 2018.

[5] B. A. Bash, D. Goeckel, D. Towsley, and S. Guha, "Hiding information in noise: Fundamental limits of covert wireless communication," *IEEE Commun. Mag.*, vol. 53, no. 12, pp. 26–31, Dec. 2015.

[6] Y. Wu and P. Li, "Security issues and solutions in wireless communications at physical layer," *China Commun.*, vol. 8, no. 5, pp. 11–19, 2011.

[7] C.-C. Shih, "Fractionalization of Fourier transform," *Opt. Commun.*, vol. 118, nos. 5–6, pp. 495–498, 1995.

[8] L. Mei, X.-J. Sha, and N.-T. Zhang, "The approach to carrier scheme convergence based on 4-weighted fractional Fourier transform," *IEEE Commun. Lett.*, vol. 14, no. 6, pp. 503–505, Jun. 2010.

[9] L. Mei, X. Sha, Q. Zhang, and N. Zhang, "The concepts of hybrid-carrier scheme communication system," in *Proc. Int. ICST Conf. Commun. Netw.*, Aug. 2011, pp. 26–33.

[10] X. Fang, N. Zhang, S. Zhang, D. Chen, X. Sha, and X. Shen, "On physical layer security: Weighted fractional Fourier transform based user cooperation," *IEEE Trans. Wireless Commun.*, vol. 16, no. 8, pp. 5498–5510, Aug. 2017.

[11] Z. Luo, H. Wang, and K. Zhou, "Physical layer security scheme based on polarization modulation and WFRFT processing for dual-polarized satellite systems," *KSII Trans. Internet Inf. Syst.*, vol. 11, no. 11, pp. 5610–5624, 2017.

[12] J. Lang, R. Tao, Q. Ran, and Y. Wang, "The multiple-parameter fractional Fourier transform," *Sci. China F-Inf. Sci.*, vol. 51, no. 8, pp. 1010–1024, 2008.

[13] L. Mei, "Weighted-type fractional Fourier transform and its applications in communication systems," Ph.D. dissertation, Harbin Inst. Technol., Harbin, China, 2010.

[14] Y. Liang, X. Da, R. Xu, L. Ni, D. Zhai, and Y. Pan, "Research on constellation-splitting criterion in multiple parameters WFRFT modulations," *IEEE Access*, vol. 6, pp. 34354–34364, 2018.

[15] E. H. German, "Transform domain signal processing study final report," Air Force, Reisterstown, MD, USA, Tech. Rep. F30602-86-c-0133, 1988.

[16] R. A. Radcliffe and C. G. Gerald, "Design and simulation of a transform domain communication system," in *Proc. MILCOM*, 1997, p. 1.

[17] C. Han, J. Wang, S. Gong, and S. Li, "Performance of the OFDM-based transform domain communication system in cognitive radio contexts," in *Proc. Int. Conf. Cognit. Radio Oriented Wireless Netw. Commun.*, Jun. 2006, pp. 1–5.

[18] C. Han, J. Wang, Y. Yang, and S. Li, "Addressing the control channel design problem: OFDM-based transform domain communication system in cognitive radio," *Comput. Netw.*, vol. 52, no. 4, pp. 795–815, 2008.

[19] X. Fang, X. Sha, and L. Mei,, "Guaranteeing wireless communication secrecy via a WFRFT-based cooperative system," *China Commun.*, vol. 12, no. 9, pp. 76–82, Sep. 2015.

[20] M. Patzold, *Mobile Fading Channels*. Hoboken, NJ, USA: Wiley, 2003.

[21] C. French and W. Gardner, "Spread-spectrum despreading without the code," *IEEE Trans. Commun.*, vol. COMM-34, no. 4, pp. 404–407, Apr. 1986.

[22] P. J. Swackhammer, M. A. Temple, and R. A. Raines, "Performance simulation of a transform domain communication system for multiple access applications," in *Proc. Mil. Commun. Conf. (MILCOM)*, Oct./Nov. 1999, pp. 1055–1059.

[23] B. Sklar, *Digital Communications*. Upper Saddle River, NJ, USA: Prentice-Hall, 2001.

[24] S. Mitra, *Digital Signal Processing: A Computer-Based Approach*. New York, NY, USA: McGraw-Hill, 2002.

[25] L. R. Rabiner, *Theory and Application of Digital Signal Processing*. Upper Saddle River, NJ, USA: Prentice-Hall, 1975.

[26] I. Budiarjo, H. Nikookar, and L. P. Ligthart, "On the utilization of embedded symbol for CCSK BER improvement in TDCS dynamic spectrum access," in *Proc. Eur. Conf. Wireless Technol.*, Oct. 2008, pp. 123–126.

[27] Y. Liang, X. Da, R. Xu, and L. Ni, "Design of constellation precoding in MP-WFRFT based system for covert communications," *J. Huazhong Univ. Sci. Technol., Nature Sci. Ed.*, vol. 46, no. 2, pp. 72–78, 2018.

[28] Y. Liang and X. Da, "Analysis and implementation of constellation precoding system based on multiple parameters weighted-type fractional Fourier transform," *J. Electron. Inf. Technol.*, vol. 40, no. 4, pp. 825–831, 2018.

[29] J. D. Foster, A. M. Berry, N. Boland, and H. Waterer, "Comparison of mixed-integer programming and genetic algorithm methods for distributed generation planning," *IEEE Trans. Power Syst.*, vol. 29, no. 2, pp. 833–843, Mar. 2014.

[30] M. H. M. A. Jahromi, R. Tavakkoli-Moghaddam, A. Makui, and A. Saghaee, "A modified genetic algorithm for solving machine-tool selection and operation allocation problem in an FMS," *J. UMP Social Sci. Technol. Manage.*, vol. 3, no. 1, pp. 491–499, 2015.

[31] L. Wang, J. Shen, J. Luo, and F. Dong, "An improved genetic algorithm for cost-effective data-intensive service composition," in *Proc. Int. Conf. Semantics*, 2013, pp. 105–112.

[32] L. Mei, Q. Zhang, X. Sha, and N. Zhang, "WFRFT precoding for narrowband interference suppression in DFT-based block transmission systems," *IEEE Commun. Lett.*, vol. 17, no. 10, pp. 1916–1919, Oct. 2013.

[33] M. E. Şahin, I. Guvenc, and H. Arslan, "An iterative interference cancellation method for co-channel multicarrier and narrowband systems," *Phys. Commun.*, vol. 4, no. 1, pp. 13–25, 2011.

[34] R. Lauer and P. Shaw, "Hybrid pseudo-random noise and chaotic signal implementation for covert communication," U.S. Patent 8 644 362 B1, Feb. 4, 2014.

[35] W. Ou, "Research on performance of low-probability-of-detection signal based on fractional Fourier domain," M.S. thesis, Harbin Inst. Technol., Harbin, China, 2016.

XINYU DA received the B.Sc. from Xidian University in 1983, the M.A.Sc. degree in communication and electronic system from the Air and Missile Defense College in 1988, and the Ph.D. degree from the School of Marine Science and Technology, NPU, in 2007. He is currently a Professor with Yanggo University and the Information and Navigation College, AFEU. His research interests include satellite communications, communication theory, signal processing, transform domain communication system, and cognitive radio.

YUAN LIANG received the B.Sc. degree in information and navigation engineering and the M.A.Sc. degree in information and communication engineering from the Air Force Engineering University, Xi'an, China, in 2012 and 2015, respectively, where he is currently pursuing the Ph.D. with the Institute of Information and Navigation. His research interests include intelligent signal processing, wireless communications, secure communications, and optimization and intelligent algorithm.

HANG HU received the B.Sc. degree in communication engineering from Xidian University, Xi'an, China, in 2010, and the Ph.D. degree in military communications from the Institute of Communications Engineering, PLA University of Science and Technology, Nanjing, China, in 2016. He is currently a Lecturer with the Information and Navigation College, AFEU. His current research interests include cognitive radio technology, cooperative communications, and signal processing in communications.

RUIYANG XU received the B.Sc. degree in automatic control engineering and the M.A.Sc. degree in information and communication engineering from Air Force Engineering University, Xi'an, China, in 2013 and 2016, respectively, where he is currently pursuing the Ph.D. with the Institute of Information and Navigation. His research interests include satellite communications, covert communications, and optimization and intelligent algorithm.

LEI NI received the B.Sc. and M.A.Sc. degrees from Air Force Engineering University (AFEU) in 2014 and 2017, respectively, where he is currently pursuing the Ph.D. degree with the Graduate School. From 2014 to 2016, he stayed at the College of Information and Navigation, AFEU, to study modern communication theory and its application in physical-layer security. His current research interests include energy harvesting, cognitive radio networks, and secure communication.

DONG ZHAI received the B.Sc. degree in electronic science and technology in 2016. He is currently pursuing the M.A.Sc. degree with the Institute of Information and Navigation, Air Force Engineering University, Xi'an, China. His research interests include wireless communications and physical layer security.

YU PAN received B.Sc. degree in electronic science and technology in 2017. She is currently pursuing the M.A.Sc. degree with the Institute of Information and Navigation, Air Force Engineering University, Xi'an, China. Her research interests include wireless communications and secure communications.